Relationship between failure height (Row) and failure depth (Bottom) just before the failure at particular distances of excavation from the toe is shown in Fig. 3. Excavation position (R-cut) of the model tests was multiplied by the centrifuge acceleration to get the real distance of excavation position from the toe. At particular distance of excavation, failure height is fixed as the slope angle of the model is constant. But as observed from the graph, failure depth decreases with the increase in the distance of excavation. This relationship is non-linear.

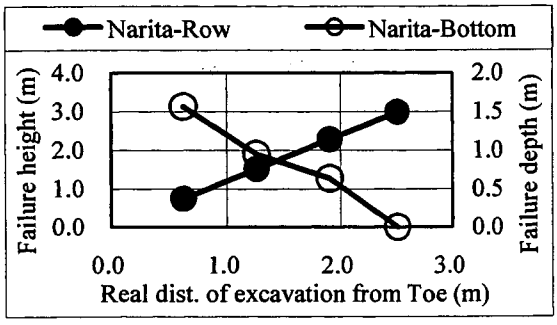

Fig. 3 Relationship between failure height and failure depth with distance of excavation from toe.

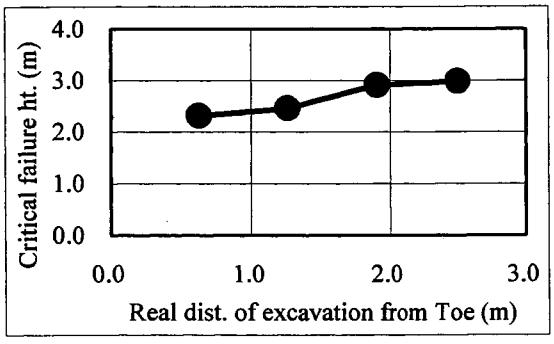

Fig. 4 Relationship between critical failure height and distance of excavation from toe.

Figure 4 shows the relationship between critical failure height and real distance of excavation position from the toe point of the slope. Critical failure height increases with the increase in the distance of excavation position from the toe. But the increment rate decreases with the increase in the excavation distance from the toe, showing the non-linear relationship. This implies that at toe or near the toe, if the trench excavation is to be made, the failure of slope might take place before it reaches the critical failure height obtained either from the normal excavation or from the theoretically calculated critical height. Henceforth, care should be taken while carrying the combined (trench) excavation.

Decrease in the critical failure height with the increase in the failure depth (trench excavation) might be thought of due to the increase in the overburden pressure (weight of extra height) behind the cut. Generally, when the toe of the slope is excavated, shear strain is accumulated near the toe. With the advancement in the combined excavation steps near the toe, overburden pressure continues to increase. Continuous increment in the overburden pressure behind the cut increases the shearing strain which finally leads to failure and slope gets failed. This is the reason why critical failure height near the toe of the slope is smaller than those at farther distances from the toe. Therefore, critical failure height during R2 cut showed the minimum value in comparison to R8 cut where the critical failure height was the maximum. From the results mentioned in Figs. 3 and 4, it could be said that the maximum value of critical failure height could only be obtained for normal excavation cases and this critical failure height decreases with the decrease in the distance of excavation position as well as with the increase in the trench excavation depth.

Figure 5 show the vertical displacement measured from LVDTs set up on the top surface of the slope for normal excavation case (R8-B0). Dashed vertical lines in the graph represent the steps of excavation. Here, elapsed time for each excavation is shown. Thus, finishing time for first step of excavation is at zero minutes. Gradual increase in vertical displacement with the increase in the steps of excavation could be observed. Comparing the amount of vertical displacement of each LVDT (D-1, D-2, D-3, D-4 and D-5), D-1 shows the maximum value and D-5 shows the minimum, D-1 was the displacement just on the crest of the slope. Large and sharp increment of D-1 displacement showed the possibility of prediction of

failure in advance if the measurement is made at the crest of the slope. Comparing the displacement of pattern of all the LVDTs in Fig. 5, it showed that whole slope moved forward and downward with the increase in the excavation steps.

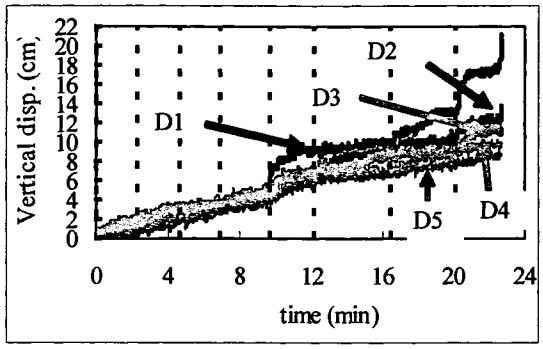

Fig. 5 Relationship between vertical displacement and elapsed time of excavation.

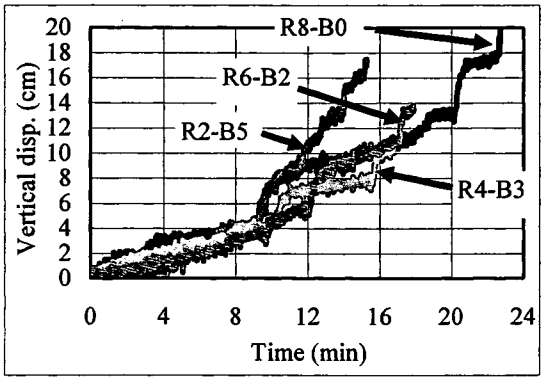

Fig. 6 Vertical displacement of D-1 with time for all the excavation cases.

In Fig. 6, vertical displacement of LVDT (D-1) for all the test cases is shown. Here also, finishing time of 1st cut was at zero elapsed time. Gradual increase in vertical displacement with the increase in the steps of excavation could be observed. Displacement pattern for each excavation cases changed after 9.7 minutes elapsed time (i.e. after 5th cut in normal excavation case). Comparing the failure time, R2-B5 took the minimum time and R8-B0 took the maximum. This shows that normal excavation takes longer time to fail than combined excavations; deeper trench excavation showing the minimum time for failure. Sharp increment in displacement pattern for R2-B5 excavation case also shows the possibility of quicker failure. From these, it could be said that while combined excavations are carried out at the toe, proper care should be taken as the possibility of failure during these excavations are higher than those at farther distances.

5. Conclusions

(1) Maximum critical failure height was obtained for normal excavation. In case of combined excavation, critical failure height (failure height + failure depth) decreases with the increase in the trench excavation depth. Reduction in the critical failure height near and towards the toe is due to the increase in the overburden pressure (weight of extra height) behind the cut.

(2) Gradual increment in vertical displacement measured on the top surface of slope showed the forward and downward movement of the slope. Sharp and maximum increment in vertical displacement of D-1 nearest to the slope crest showed possibility of failure prediction in advance.

(3) Failure time for combined excavation (normal + trench) is smaller than that for normal excavation; combined excavation made nearer to the toe showed the minimum time to fail. Also, displacement pattern nearer to the toe showed sharp increment.

6. Acknowledgement

This work is partially carried out under the Health and Labor Sciences Research Grants of Ministry of Health, Labor and Welfare.

References

1). Tamrakar, S.B., Toyosawa, Y., Itoh, K. & Kusakabe, S. 2005. Failure mechanism of slopes in the centrifuge using In-flight excavator, International symposium on Landslide Hazard in Orogenic Zone from the Himalaya to Island Arc in Asia, Kathmandu, Nepal, 25-26 September 2005: 255-264.

2). Toyosawa, Y., Horii, N., & Tamate, S. 1998. Deformation and failure behavior of anchored retaining wall induced by excessive excavation in centrifuge model tests, Research Reports of the National Institute of Industrial Safety (NIIS-RR-97):35-46.

Factors affecting tensile strength measurement and Modified Tensile Strength measuring apparatus for soil

Surendra Bahadur Tamrakar[(i)], Toshiyuki Mitachi[(ii)] and Yasuo Toyosawa [(iii)]

i) Research Resident "Rank A", NIOSH, Institute of Industrial Safety, Tokyo, Japan.
ii) Professor, Hokkaido University, Hokkaido, Japan.
iii) Senior Researcher, NIOSH, Institute of Industrial Safety, Tokyo, Japan.

Abstract

In this paper tensile strength measuring apparatus developed by Tamrakar et. al (2005) was used to measure the tensile strength of one dimensionally consolidated saturated NSF-clay and statically compacted unsaturated mixtures of NSF-clay, CFP-silt and Toyoura-sand. Tensile strength (q_t) obtained from the tensile tests were compared with the unconfined compressive strength (q_u). It was observed that the ratio, q_u/q_t lied within the range of 2 to 3 for saturated NSF-clay and 4 to 16 for compacted mixtures. Effect of specimen thickness within the tensile mold, number of compaction layers and tensile pulling rates on the tensile strength were also examined. Comparing the specimen thickness within the tensile mold, it was found that the specimen having 5 cm thickness gave the minimum value. Also, tensile strength increased with the increase in the number of compaction layers. As in other shear strength, increment in the tensile strength was observed beyond tensile pulling rate of 0.34 mm/min. But below this pulling rate also, some increments were observed.

Introduction

Most of the vertical slopes get failed with the development of tensile crack on the top of the slope. Also, many earth dams, embankments, pavements, etc. where soil layers are compacted, are failed due to the development of tensile cracks. Prediction of probable position and depth of tensile crack is necessary to protect the property and loss of lives of workers at the construction site. In order to explain the position and depth of tensile crack, an accurate measurement of tensile strength of soil is necessary. Very few researches (e.g. Suzuki et al., 1998; Yao et al., 2002 and Ono et al., 2003) have been made to measure the tensile strength of soils having lower tensile values. Recently, Nahlawi et. al (2004) and Tamrakar et. al (2005) have introduced new tensile strength measuring apparatus which measures the tensile strength directly. One developed by Nahlawi et. al (2004) could be mainly used for compacted clayey and stiff soils only whereas the one developed by Tamrakar et. al (2005) seems to be easy to use and simple to handle and could be used for both compacted unsaturated and highly saturated soils.

Tamrakar et. al (2005) measured the maximum tensile strength of Kanto loam around 50~60% of water content and showed the ratio of unconfined compression strength and tensile strength around 12.5 which varied with the water content. They also showed the effect of amount of finer particles and their size on tensile strength. Possible measurement of tensile strength for saturated NSF clay was also shown.

In this paper, tensile apparatus (type-A tensile mold) developed by Tamrakar et. al (2005) was used to measure the tensile strength of saturated and unsaturated soils. Also, the effect of number of compaction layers, thickness of the specimens and tensile pulling rate on the tensile strength was studied. Unconfined compression tests were also performed to compare their values with tensile strength.

Test Apparatus

Tensile test apparatus shown in Photo 1 consists of horizontal platform upon which apparatus box having two halves; fixed box and movable box, is placed. Inside this box, two tensile molds are

placed. The inner shape of this mold is like "C" structure and it holds the specimen. Two molds are screwed to the apparatus boxes separately. One box of the apparatus is fixed to the horizontal platform while the other box can move freely on the horizontal platform. To reduce the friction, linear sliding roller is placed between the movable box and platform. Movable box is pulled away in horizontal direction until the soil specimen fails in tension with tensile crack appearing at the middle of the specimen where two halves of the mold is attached. Load cell placed between the movable box and motor axis measures the tensile load. This tensile load divided by the area of the tensile crack perpendicular to horizontal pulling direction, gives the tensile stress. These molds can be easily changed as they are connected to the main apparatus by the screws only. The total surface area of this mold is 38.5 cm^2. The minimum width at the constricted section of this mold is 3 cm and the depth is 5 cm.

The apparatus box along with the mold and platform can be completely separated from the motor for preparing the specimen before the test. Compacted soil specimen is prepared within this mold by direct static compression. Once the specimen is ready within the mold for the test, then it is connected to motor shaft. Between the motor shaft and movable apparatus box, there are some attachments where load cell is kept.

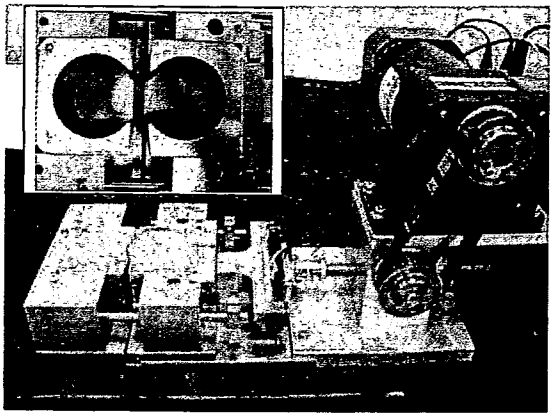

Photo 1. New tensile strength measuring apparatus (inset : tensile molds) (Tamrakar et. at (2005).

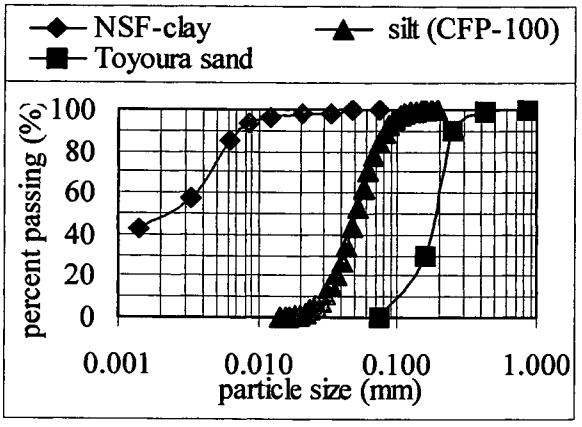

Fig. 1. Grain size distribution curves.

Materials and Specimen Preparation

Kanto loam, NSF-clay and the mixtures of NSF-clay, CFP-silt and Toyoura-sand were taken as test materials. NSF-clay is commercially available clay which consists of Pyrophylite, CFP-silt (100) is crushed form of Silica sand and Toyoura-sand is also commercially available standard Japanese sand. Grain size distribution curves and index properties for these soils are shown in Fig. 1 and Table 1. Now onwards, NSF-clay, CFP-silt and Toyoura-sand are represented by clay, silt and sand, respectively. For saturated test specimen, consolidated clay specimens were used where as mixtures of clay, silt and sand in different proportions were used for unsaturated compacted specimens. Table 2 and 3 show the proportions and test conditions for different mixtures.

Before preparing the specimens, at first, tensile molds were fixed into the apparatus box and screwing was done between the movable box and apparatus horizontal plate so that movable box would be fixed. To reduce the friction between the specimen and the inner wall of the tensile mold, thin film of grease was applied over its inner surfaces. After the insertion of the consolidated specimen in case of saturated specimens or after the completion of compaction in case of compacted specimens into the tensile mold, load cell is set up towards the pulling side of mold box. Finally, the screws which are earlier fixed to prevent the movement of movable box of the apparatus are un-screwed

Table 1 Properties of test materials

Materials	density	dry density		w_L	w_P
	soil solid	max.	min.		
	g/cm^3	g/cm^3	g/cm^3	(%)	(%)
NSF-clay	2.78			55.1	30.6
silt (CFP-100)	2.66	1.59	1.17		
Toyoura sand	2.64	1.65	1.34		

Saturated specimens were prepared by pre-consolidating the slurry of the clay material in a separate, special consolidation mold. Two-way drainage with one dimensional consolidation was done. Once the consolidation was over, consolidation mold with consolidated specimen was placed over the tensile mold. Centering of molds was done by guiding support screws which were attached to the fixed portion of the apparatus box. By pushing the shaft of the consolidation mold slowly, consolidated specimen was allowed to insert into the tensile mold. Once the full depth (5 cm) insertion was completed, then the specimen was cut and its upper surface was trimmed.

Table 2 Test mateials for mixtures of clay, silt and sand.

dry density	NSF-clay	CFP-silt	Toyoura-sand	q_u	q_t	q_u/q_t
(g/cm^3)	%	%	%	(kPa)	(kPa)	
1.50	25	-	75	21.1	3.2	6.5
	40	-	60	55.9	6.6	8.4
	50	-	50	74.4	7.8	9.5
	60	-	40	79.1	8.6	9.2
	75	-	25	131.3	12.1	10.9
1.50	25	75	-	64.3	6.9	9.3
	40	60	-	100.0	8.4	11.9
	50	50	-	97.8	8.5	11.5
	60	40	-	132.2	10.3	12.9
	75	25	-	182.2	11.7	15.5
1.40	-	25	75	6.6	1.4	4.6
	-	40	60	12.9	2.2	6.0
	-	50	50	16.4	2.7	6.1
	-	60	40	18.7	3.0	6.2
	-	70	30	26.7	3.9	6.9

In case of compacted specimens, at first, materials were thoroughly mixed with required distilled water and kept in an air tight plastic bag and sealed so that water was uniformly distributed throughout the materials. Specimens were prepared either under constant stress or under constant dry density conditions. In both the conditions, compacted specimens were prepared by directly and statically compressing the prerequisite amount of soil kept within the tensile mold of the apparatus, using bellophragm cylinder. Collar was generally placed over the tensile mold to prevent falling out of soil from the mold. Specimens were compacted keeping the dry density, water content and thickness of the specimens constant. Thickness, number of compaction layers and tensile pulling rates were varied depending upon the test conditions.

Table 3 Mixing propertions and Testing conditions for clay ~ sand mixtures.

Specimens	Mixing ratio	w	Controlled			Testing Conditions
			dry density	compaction stress	dry density	
	(by wt.)	(%)	(g/cm^3)	kPa	(g/cm^3)	
clay~sand	3:1	10.0	1.50			No. of layers[(1)]
clay~sand	3:1	10.0	1.50			Thickness[(2)]
clay~sand	1:3	10.0		200	1.54	Pulling rate[(a)]
clay~sand	3:1	10.0		200	1.26	
clay~sand	3:1	10.0	1.50			Pulling rate[(b)]
clay~sand	1:3	10.0	1.50			

[(1)] one, two and four layer-compaction, [(2)] 1.25, 2.5, 3.75 and 5 cm

[(a)] 0.01, 0.09 and 0.34 and 0.88 mm/min, [(b)] 0.17, 0.34 and 0.88 mm/min

In case of unconfined compression test, saturated specimens were prepared by pre-consolidating the clay specimens in an ordinary consolidometer where as unsaturated compacted specimens were prepared in a normal splitting mold either under constant stress or constant dry density condition. Generally, one layer compaction was done. But to see the effect of numbers of layer of compaction, some specimens were prepared with one, two, three, four, five and ten layers.

Test Conditions

Tests in which specimen thickness was maintained at 5 cm with one-layer compaction and pulled under 0.34 mm/min tensile pulling rate, were considered as Reference tests. All the tests of saturated specimens are reference tests. Saturated specimens of clay were prepared under 100, 200 and 300 kPa. Water content, density, degree of saturation, etc. is shown in Table 4.

In case of unsaturated specimens, test conditions were changed depending upon the type of tests. Mixtures of clay, silt and sand specimens were prepared by mixing them in different proportions as shown in Tables 3 and 4. Specimens were compacted keeping their dry density, water content and specimen thickness constant. In case of tests where the effect of specimen thickness was studied, specimens were prepared by one-layer static compaction and they were pulled with 0.34 mm/min. In this case specimen thickness varied from 1.25 to 5 cm. Similarly, where the effect of number of layers of compaction was studied, specimens were prepared with one-layer, two-layers, three-layers and four-layers of static compactions, keeping the overall specimen thickness to be around 5 cm and pulling them under 0.34 mm/min. In case of the tests where the effect of tensile pulling rate was studied, specimens were prepared by one-layer static compaction with specimen thickness of 5 cm. In this case, tensile pulling rate was varied from 0.09 to 1.75 mm/min.

ble 4 Saturated sol specimens conditions and test resu

Specimen type	NSF-clay				
Preconsolidation pressure	100	200	200	300	300
Soil unit weight γ_t (kN/m^3)	27.23	27.23	27.23	27.23	27.23
Water content w (%)	55.51	45.03	46.65	45.61	42.84
Degree of saturation S_r (%)*	98.40	97.20	96.70	98.75	96.00
q_t (kPa)	13.54	18.34	20.64	25.35	27.04
q_u (kPa)	29.81	52.81	52.81	77.12	77.12
q_u/q_t	2.20	2.88	2.56	3.04	2.85

* for tensile test

Unconfined compression test for saturated specimens were prepared by trimming the pre-consolidated specimens whereas unsaturated compacted specimens were prepared using ordinary splitting mold. Other than those for the effect of number of compacted layers, all the compacted specimens were prepared by one-layer static compaction using bellophragm cylinder. Other conditions such as dry density and water content were kept same as those for tensile compacted specimens. Compacted layers were prepared with 1, 2, 3, 4, 5 and 10 layers. Compaction time allowed for each layer was around 1 minute. The height and depth of specimen for both saturated and unsaturated cases were 10 cm and 5 cm, respectively. Unconfined compression tests were conducted at constant displacement rate of 0.1 mm/min.

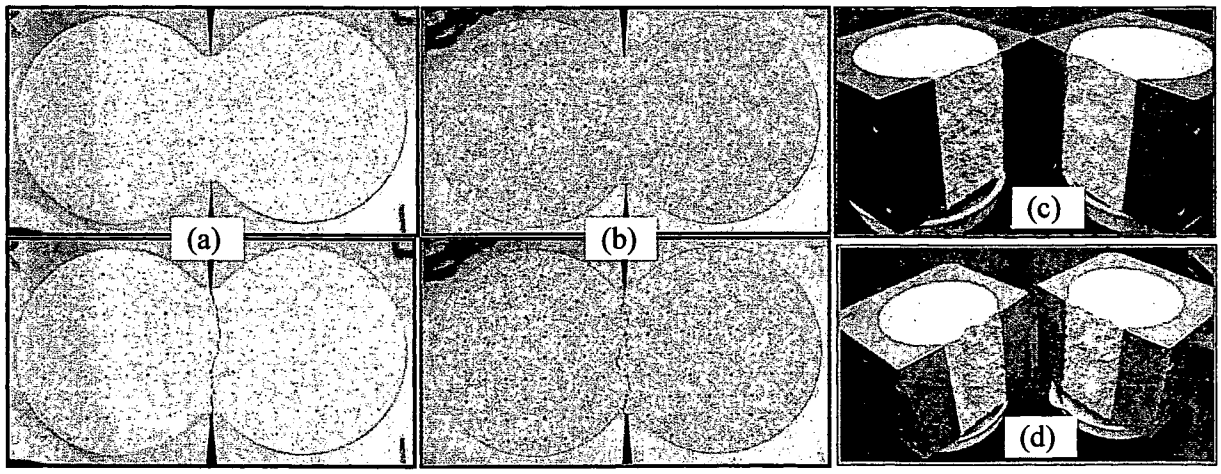

Photo 2 Photographs before and after the tensile failure. (a) and (c) clay ~ sand mixture (3:1) and (b) and (d) clay ~ sand mixture (1:3).

Results and Discussions

Photos 2(a) and (b) showed the photographs before and after the tensile failure tests for clay~sand (3:1) and clay~sand (1:3), respectively. Clear and straight tensile crack (failure line) could be seen. In Photos 2(c) and (d), failure planes (tensile crack plane) after the tests were shown. Clear and smooth failure surfaces could be seen.

Tensile stress ~ displacement curves obtained for the saturated specimens of clay (pre-consolidated under 100, 200 and 300 kPa) are shown in Fig. 2. As shown, with the increase in consolidation pressure, there is increase in tensile strength. Small variation in the test result might have occurred either during the transferring of the consolidated specimen from the pre-consolidometer to tensile mold or during the trimming of the specimen surface. In addition, variation in the water content (degree of saturation) or the friction between the inner wall of the consolidation mold and slurry material during the pre-consolidation might also have affected small change in their strength. Henceforth, proper attention must be paid during the specimen preparation. Stress ~ displacement curves for clay~silt~sand (1:1:1) obtained from tensile test and unconfined compression tests were shown in Figs. 3(a) and (b), respectively. Clear peak for tensile stress as well as unconfined compressive stress could be seen. Here, tensile stress measured was shown in negative value. From now onwards, tensile strength values would be shown as positive values.

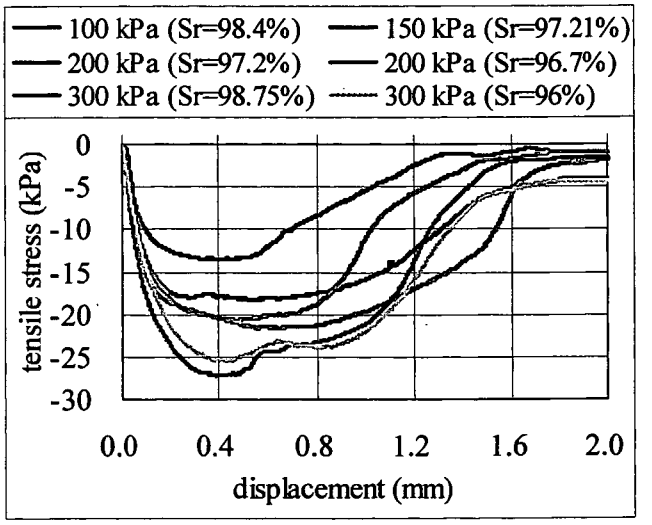

Fig. 2. Tensile stress ~ displacement curves for consolidated NSF-clay.

In Table 4 shows the tensile strength and unconfined compression strengths obtained for saturated specimens. Increase in both tensile and unconfined compression strengths with the increase in the consolidation pressure could be seen. It was observed that the ratio of q_u/q_t for saturated clay varied from 2~3. Another type of NSF-clay used by Tamrakar et al. (2005) had shown the average ratio as 6. All the test specimens shown in Table 4 have more than 93% of degree of saturation. Degree of saturation (S_r) shown in the Table 4 was calculated by using unit wet of soil solid, total weight of the specimen inside the tensile mold and the water content of the specimen after failure. As it is difficult to measure the area of the specimen directly, the total area of the specimen was considered to be same as that of the tensile mold. Thickness of the specimen was measured once the trimming was done after transferring the consolidated specimen into the tensile mold. It was assumed that the specimen tightly fits into the mold. Ratio of q_u and q_t for clay~silt~sand (1:1:1) specimen was found to be 8.6. In Tables 2 and 3, tensile and unconfined compression strengths measured for different mixtures are shown. It could be seen that the ratio of q_u/q_t for the unsaturated mixtures varied from 4 to 16. Tamrakar et al. (2005) had also measured the similar ratio of q_u/q_t for Kanto loam which varied from 10 to 13 (Tamrakar et al., 2005).

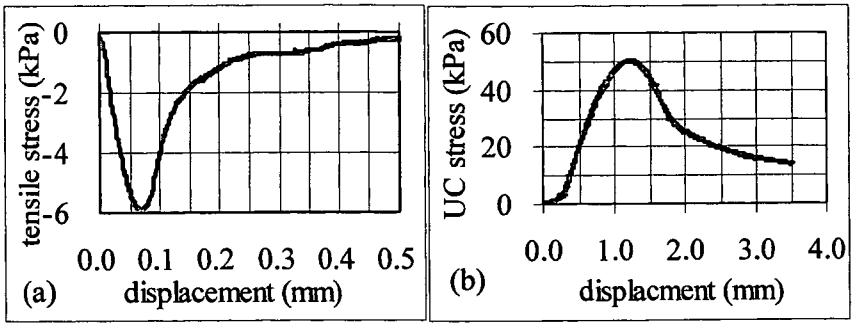

Fig. 3. Stress ~ displacement curves for clay ~silt~sand (1:1:1) mixture (a) tensile test and (b) unconfined compression test.

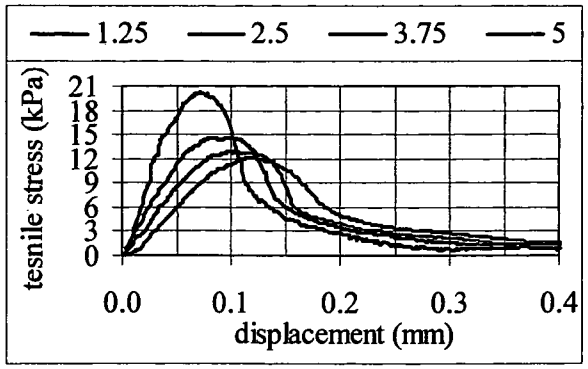

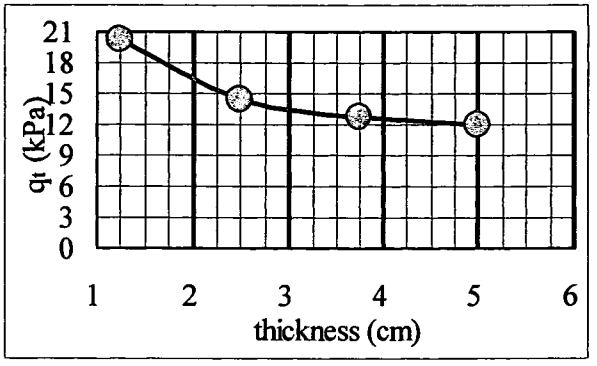

Fig. 4 Effect of thickness on q_t (a) Stress ~ displacement curves and (b) tensile strength.

Effects of specimen thickness are shown in Figs. 4. Here, tensile strength values for different specimen thicknesses are shown. Decrease in the tensile strength with the increase in the specimen thickness could be seen. Specimen having 5 cm thickness, i.e., the thickness of tensile mold, showed the minimum tensile strength. Here, specimens were compacted only once for all the thicknesses. Therefore, uniformity in the density is more in case of specimen which had the minimum thickness. Irrespective of specimen thickness, tensile pulling for each test was done from the mid-height of the tensile mold. With the change in the thickness, resultant pulling direction might have changed, hence affecting the strength.

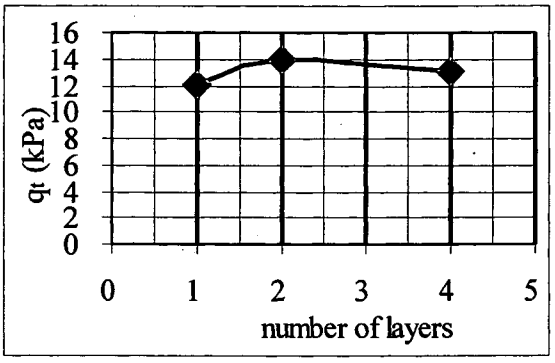

Fig. 5. Effect of number of compaction layers on qt for clay ~ sand mixture (3:1).

The effect of number of layers of compaction to tensile strength is shown in Fig. 5. During this test, 5 cm thick specimens were prepared by compacting predetermined amount of specimen within the tensile mold in one-layer, two-layer, three-layer and four-layer. Clay-sand mixture (3:1, w=10% and rd=1.5 g/cm3) showed the increment in tensile strength with the increase in the number of compaction layers. One-layer compaction gave the minimum value than those obtained for two, three and four-layer compaction. With the increase in number of compaction layers, more uniformity of density through out the specimen takes place and this will increase the strength of the specimen. Similar test result was seen in case of unconfined compression test shown in Fig. 6 where test specimens were prepared by statically compacting the same amount of clay-sand mixture (1:3, w~10%, compaction pressure 50, 100 and 200 kPa) with 1, 2, 3, 4, 5 and 10 layers. As shown in Fig. 6, at the beginning, sudden increase in q_u strength was seen but the rate of increment decreased with the increase in the number of layers. As obvious, with the increase in number of layers of compaction, more uniformly dense specimens were obtained which makes the bonding between the soil particles more strong and hence, strength is increased.

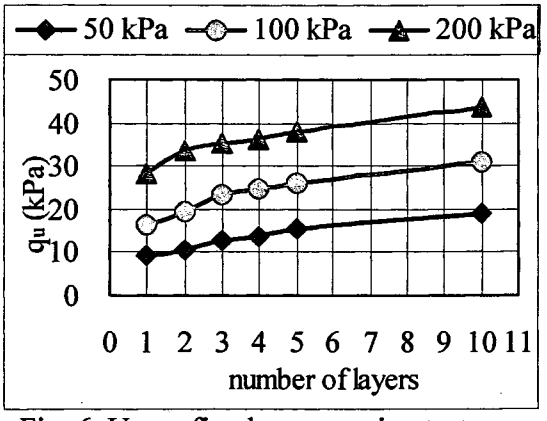

Fig. 6. Unconfined compression test results for clay ~ sand mixture (3:1).

Figure 7 shows the tensile strength test results of different soils conducted at different pulling rates which varied from 0.01 to 1.75 mm/min. In Fig. 7(a) clay-sand mixtures (1:3 and 3:1) prepared under 200 kPa were shown where as in Fig. 7(b) same soil specimens prepared under constant dry unit were shown. Comparing the tensile strength of each specimen with respect to tensile pulling rate, variation in the strength with the change in the pulling rate could be observed

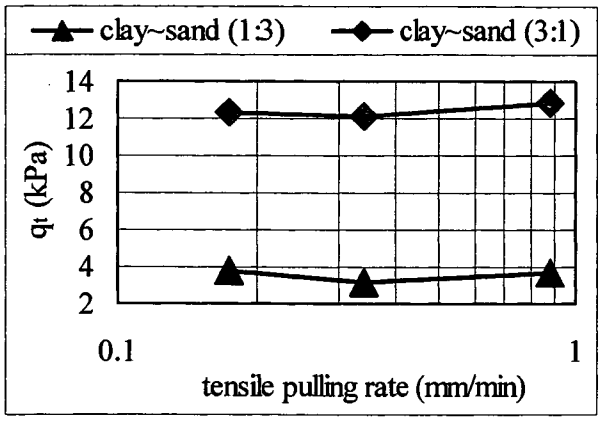

Fig. 7(a). Effect of tensile pulling rate on tensile strength (under controlled pressure).

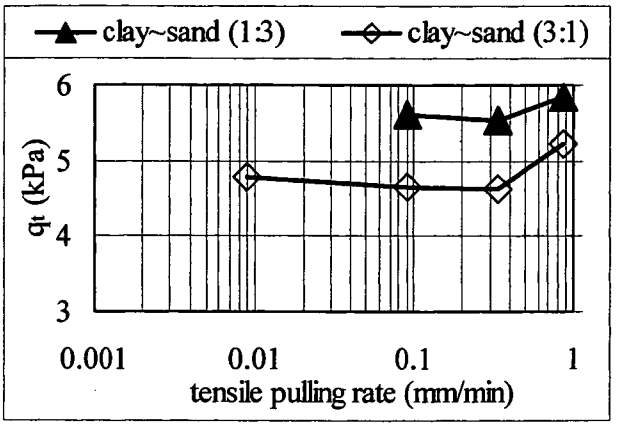

Fig. 7(b). Effect of tensile pulling rate on tensile strength (under controlled dry density).

for all types of soil specimens. It was observed that the tensile strength measured in the range of 0.1 to 0.34 mm/min pulling rate gave the minimum value. In contrary to this, tensile strength measured at the higher and lower tensile pulling rates than 0.1 mm/min showed larger values. This difference in the tensile strength might have occurred while pulling the specimens where soil particles are attached to each other either by suction or internal bonding or cohesion. Tamrakar et al. (2005) had discussed about the relationship between the tensile strength and suction to some extent. Effect of suction at higher and lower tensile pulling rates are yet to be studied. Increment in the tensile strength at higher tensile pulling rate is obvious as in any other shear strength. One reason for the increment at very low pulling rates might be due the dryness on the surface of the specimen as it takes very long time. Other reasons are yet to study.

Conclusions

From the tests conducted for saturated and statically compacted unsaturated soils, following points could be concluded;

1. Stress-displacement curves obtained for both saturated and compacted unsaturated specimens show the possibility of measuring tensile strength with the apparatus used here.

2. Ratio of unconfined compression strength and tensile strength (qu/qt) for NSF-clay was found to be 2~3. For unsaturated soils this ratio varied from 4 to 16 depending upon the type and water content of the soil.

3. From the test results of clay-sand mixture (3:1), it was found that 5 cm thick specimen gave the minimum tensile strength in comparison to other specimens having thickness smaller than 5 cm. Therefore, it is recommended to pull the specimen from its mid-height.

4. Effect of number of layers of compaction (one-layer, two-layer and four-layer) on tensile strength was also studied. It was found that with the increase in the number of compaction layers, there was increase in tensile strength. Similar result was obtained in case of unconfined compression test also. Increment in the strength might have occurred due to increase the uniformity of density distribution throughout the specimen.

5. Effect of tensile pulling rate for variety of unsaturated soil specimens was carried out. It was found that with the increase in the tensile pulling rate beyond 0.34 m/min, tensile strength also increases. But below this pulling rate also, some increments were observed.

Acknowledgements

This research is partially carried out under the Health and Labor Sciences Research Grants of Ministry of Health, Labor and Welfare, Japan.

References

Nahlawi, H., Chakrabarti, S. and Kodikara, J., 2004, "A direct tensile strength testing method for unsaturated geomaterials," Geotechnical Testing Journal, Vol. 27, No. 4, pp. 356–361.

Ono, N., Mochizuki, A., Kurosaki, H. and Ueno, K., 2003, "Trial tests with compressive and tensile strength measuring apparatus," 58th Annual meeting of Japanese Society of Civil Engineers, pp. 337–338 (in Japanese).

Suzuki, T., Umei, T. and Sunaga, F., 1998, "A research on the tensile strength of cement treated soils," 53rd Annual meeting of Japanese Society of Civil Engineers, pp. 600–601 (Japanese).
Tamrakar, S.B., Toyosawa, Y., Mitachi, T. and Itoh, K., 2005, "Tensile strength of compacted and saturated soils using newly developed tensile strength measuring apparatus," Soils and Foundations, Vol. 45, No. 6, pp.103-111.

Tamrakar, S.B., Mitachi, T., Toyosawa, Y. and Itoh, K., 2005, "Development of a New Soil Tensile Strength Test Apparatus," Geo-Frontiers 2005, GSP 138 Site Characterization and Modeling, ASCE.

Yao, S., Masui, T. and Ito, A., 2002, "The relationship between tensile strength and the state of water in Kaolin clay," 47th symposium on Geotechnical symposium, pp. 127–132 (in Japanese).

International Geotechnical Symposium "GEOTECHNICAL ENGINEERING FOR DISASTER PREVENTION & REDUCTION"
July 25-27, 2007
Yuzhno-Sakhalinsk, Russia

Possible use of Tilt-sensor for failure movement and failure plane just before slope failure

S. B. Tamrakar[1], Y. Toyosawa[1], T. Mitachi[2], K. Itoh[1], K. Takashi[3]

[1]Construction Safety Research Group, Japan National Institute of Occupational Safety and Health, Tokyo, Japan
[2]Graduate School of Engineering, Hokkaido University, Hokkaido, Japan
[3]Akebono Brake Industry Co. Ltd., Saitama, Japan

Abstract

In reference to SSC type tilt sensor (Tamrakar et. al, 2005), SL type tilt sensor was designed here by placing three sets SSC type of tilt sensor, separately on each attachment table which are jointed to one single, straight and long flexible plastic plate. Depending upon the position of SSC on SL, they are called as SLU (uppermost), SLM (middle) and SLL (lowermost). As SL type tilt sensors are inserted into slope during excavation, they could measure not only the movement of upper layer of the slope but also inner layers. Applicability of SL sensor was tested in the laboratory by conducting a small scale full size test (60 degree angle) with River sand. Manual excavation around the lower part of the slope was continued till failure occurred. Sharp increment in the tilt angle just before the failure could be observed for each set of tilt sensor inserted on slope surface and slope top.

Keywords: *tilt sensor, failure, slope movement, small scale full size test.*

1 Introduction

Measurement of the displacement and deformations of ground surfaces are generally carried out at the construction sites where embankment or excavation and reclamation works are carried out. Most of the measurements are made to find the amount of settlement or movement along vertical and horizontal directions. But in case of construction works where excavation of slope is made either for retaining wall construction or for the stability of slopes, sometimes movement of slope takes place all of sudden taking the live of workers and damaging the property around the site. To prevent the accident, constant observation of slopes is important. But in general at the beginning movements are very small which is difficult to distinguish by naked eyes and just before the failure, movement becomes fast which makes no time to workers for the escape. Many researches have been presented various methods of measuring the movement of the slope. Most of them are either difficult of set up or expensive of to use in wide working field. Recently, Tamarkar et. el (2006) have developed small size compact type (SSC) and stand alone (SA) type tilt sensors which could be used in the field. These sensors could measure the movement of slope during and just before the failure. But SSC type tilt sensors are generally placed on the slope surface and slope top only. They could measure only the movement of top surface of the slope. During the slope failure, some kind of failure plane is generally seen where upper layer of slope slides over the sliding plane over the lower layer. It would be better if failure plane could be predicted in advance.

In this paper, possibility of measurement of movement of inner layers of the slope including the upper layer was tried using the SSC type tilt sensors during and just before the slope was tried. This was done by conducting small size full scale test within the laboratory so that it could be applied in the real excavating field in the future.

2 Tilt sensors

Tilt sensor used here consists of either one or two sets of highly sensitive accelerometer (Fig. 1(a)). Highly sensitive accelerometer is light in weight and small in size (9x5x1 1mm). It is made of three silicon layers; outer two layers act as fixed electrodes and inner middle one layer acts as movable electrode as shown in Fig. 1(b). When the accelerometer position is changed (tilted), this movable electrode moves so that distance between the fixed and movable electrode changes. With the change in distance between the electrodes, output capacitance changes and it further changes the output voltage. By calibrating this output voltage with the change in tilt angle, one can measure the tilting angle. The sensitivity of accelerometer used here is 100mV/deg with ±20° measurement range. Thermal sensitivity is around 10 mV/°C. General outline of the tilt sensor is shown in Fig. 1(c) (Tamrakar et al,.2006). This is a small size compact type (SSC) tilt sensor in which two sets of accelerometers were placed in such a way that it could measure both ± tilt angles along X and Y direction. These are placed above the base plate which is supported by the tubular hollow pipe cut into an

angular shape so that it can be easily inserted into the soil without propagating the crack (with less disturbance). SSC type tilt sensors are directly inserted into the slope (as well as slope top). In this case, top portion of the sensor lies well above the slope ground. With this sensor, tilt angle of the outer layer of the slope could only be measured.

In this research, as the movement of inner layers of the slope are tried to measure. Therefore, SSC type tilt sensor is little modified. Only the top portion of SSC type tilt sensor which consists of two accelerometers is used. These are attached to a flexible and thin acryl plate with the help of small attachment tables. In this paper, this type of tilt sensor is named as SL type tilt sensor and depending upon the positions of table on the acryl plate, each group of sensor are termed as SLU (for the uppermost), SLM (for the middle) and SLL (for the lowermost). Here, in one model test, two attachments are only made (only SLU and SLL) where as in another test three attachments are made (SLU, SLM and SLL). Distance between SLU and SLM is 15 cm. Therefore, SLU and SLL are 30 cm apart. In Fig. 1(d), SL type tilt sensor with three sets of sensors is shown. In the experiment here, both SSC type and SL type tilt sensors were used so that comparison between could be made.

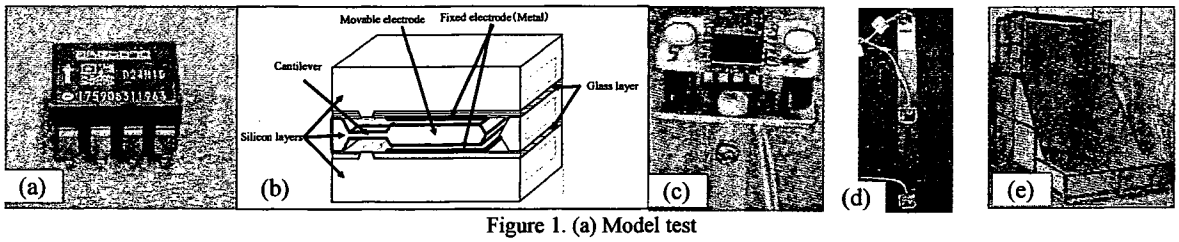

Figure 1. (a) Model test

3 Small Size Full Scale Test

To test the applicability of SL type tilt sensor during the excavation of lower portion of the slope, a small size full scale test was done in the laboratory using a test box shown in Fig 1(e).

3.1 Test Box and Model Slope

To make the model slopes within the laboratory, test box made up of wooden planks shown in Fig. 1(e) was used. This test box has two sections; lower (1.35mx 2.7m x 1.32m) and upper (1.35m x 1.2m x 0.88m). These sections facilitate in modeling the slopes with different slope heights and slope angles. At the beginning, model box is surrounded from all the sides by the wooden planks except the upper face. River sand mixed with water (around 8%) was poured into the text box. Then leveling and compaction were done manually in layers. These processes are repeated until both the sections were filled up. To cut the fill up into desired slope, wooden planks from the front and side walls were removed carefully. Slope of desired angle and height was then made by trimming. Here, thickness at the bottom was kept around 30cm so that trench excavation is possible. Two types of slope made are in Figs. 2(a) and 2(b) for shorter height (SH) and longer height (LH), respectively. At first, SH slope was made and once it was failed, then LH slope was made behind it. Properties of the model slopes are shown in Table 1. Water content and bulk density along the depth of the model slopes measured were varied to some extent.

Table 1. Properties of model tests.

Slope type	Shorter height (SH)	Longer height (LH)
Water content (%)	7.18~8.38	7.00~8.00
Bulk density, ρ_t (g/cm^3)	1.59~1.66	1.59~1.66
Slope angle (°)	60	60
Slope height (cm)	98.00	190.50
Back fill	Yes	No
No. of cuts	10	13
Total failure time (minute)	70.50	94.50

3.2 Instrumentation Set Up and Excavations

In order to measure the movement of the slope surface and slope top, two types of tilt sensors (SSC and SL types) mentioned above were used along with the laser sensors. SL type tilt sensors (SL1, SL2 and SL3) are used to measure the tilt angles of upper and inner layers where as SSC type tilt sensors (SSC1, SSC2 and SSC3) are used to measure the tilt angle of upper layer of slope only. To set up the SL type tilt sensor, at first, long hole was drilled at the desired position with less than 30cm depth and then the SL tilt sensor was inserted into that hole as shown in Fig. 2(c) and 2(d). Spaces between the SLL and SLM, and SLM and SLU are filled up by sand. Slight tamping and compaction was done. Insertion is stopped when SLU just lies on the slope level. In case of SSC, tubular pipe attached to its base is inserted on to the slope ground so that its accelerometers lie well above the ground level. Approximate position of each sensor is shown in Fig. 3. Schematic diagrams for these tilt sensors are shown in Figs. 4(a) and 4(b). Laser sensors are used to measure the movement of the slope surface (S1, S2 and S3) and deformations of slope top. In case of slope top, vertical

displacement is measured by V1 and V2 laser sensors and horizontal displacements by H1 and H2 laser sensors. In Figs. 3(a) and 3(b), set up position for each sensor in each type of test are shown.

After the set up of instruments, manual excavations were started from the lower portion of the slope manually, starting the excavation from the center and moving away from the center towards left and right sides of the slope. Both toe and trench excavations were made. Sequences of excavation carried out were shown in Figs. 4(c) and 4(d) where each step was represented by numbers; 1, 2, 3, 4, etc. In both the slopes, at first toe excavations were carried out and which was later on followed by trench excavations. Width of each toe excavation was about 5.5cm and the depth of each trench was maintained at 10cm except for 10th cut of SH slope and 13th cut of LH slope. About 5 minutes of waiting time was allowed between each excavation to see the movement of the slopes (both slope and top) after the excavation. Excavation was continued until failure of slope took place. For SH slope, under-cutting was done at the 10th cut. Similarly, for LH slope, trimming of excavated surface was done at 13th cut.

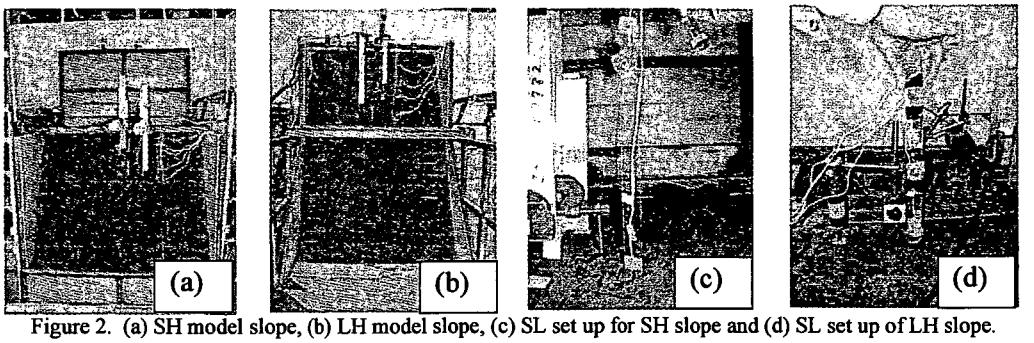

Figure 2. (a) SH model slope, (b) LH model slope, (c) SL set up for SH slope and (d) SL set up of LH slope.

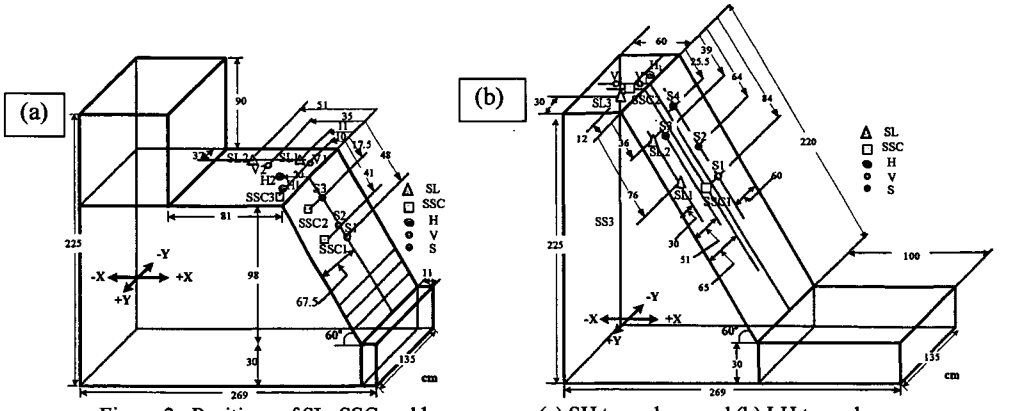

Figure 3. Positions of SL, SSC and laser sensors (a) SH type slope and (b) LH type slope.

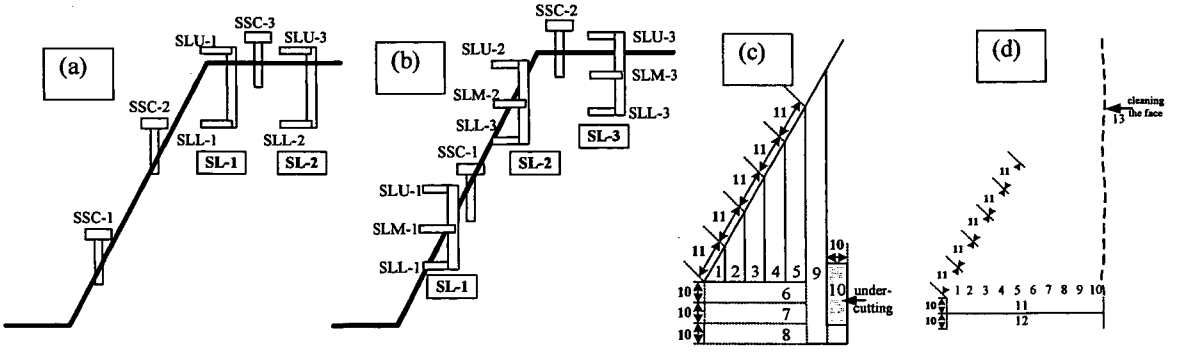

Figure 4. SL and SSC type tilt sensors for (a) SH slope, (b) LH slope and excavation steps for (c) SH slope and (d) LH slope.

4 Test Results and Discussions

In Figs. 5(a) and 5(b), slopes after failure are shown. Failure within the slope was seen in case of SH slope, especially towards the right side of the slope while carrying out the under-cutting of the slope toe at 10th cut. Failure was seen after 70 minutes. Failure

within the slope as well as toward the right side of the slope might have occurred due to small variation in the water content and unit weight within the model slope. In case of LH slope, failure was occurred while trimming the excavated wall of the slope at 13th cut. Failure of the slope was seen after 94.5 minutes. In contrary to SH slope, failure of whole slope was observed in this case except a small portion at the top right corner which might be due to the variation in water content and unit weight within the slope. Here, failure was extended in the slope top also; about 12 cm width from the crest of the slope. Therefore, LH showed deeper depth of failure area than SH slope. Comparing the two slopes, it showed that SH slope was failed when more than 87% of its slope length (surface) was excavated along with the trench. But SL slope was failed when 50% of its slope length was excavated along with the trench. This shows that the with increase in the slope length (slope height), the possible width of toe excavation decreases which is obviously due to the pressure behind the cut that increases with the slope length.

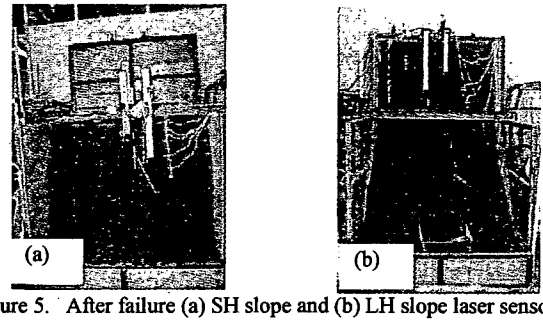

Figure 5. After failure (a) SH slope and (b) LH slope laser sensors.

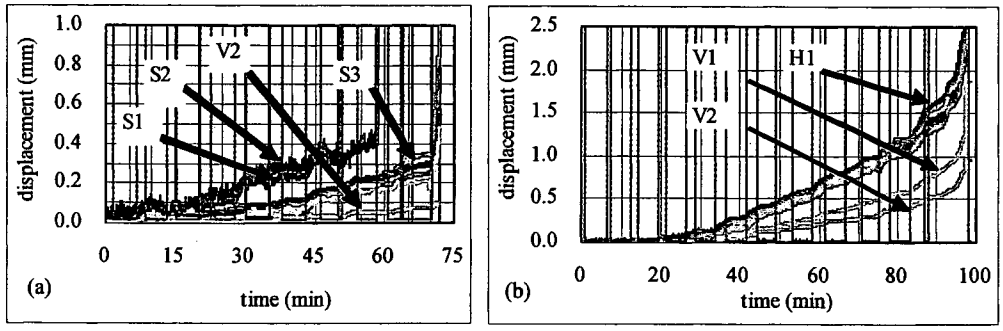

Figure 6. After failure (a) SH slope, (b) LH slope and laser sensors measurement (c) SH slope and (d) LH slope.

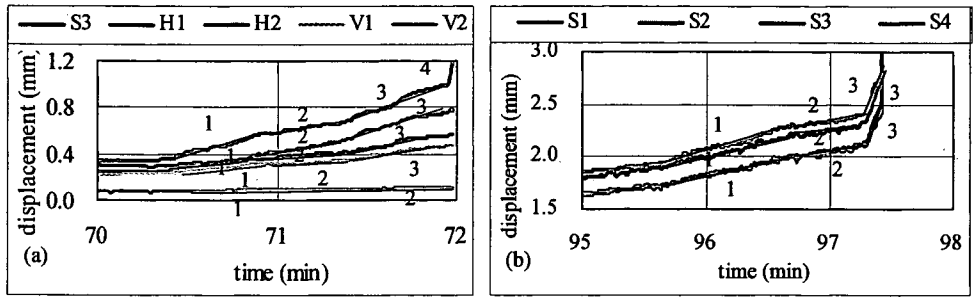

Figure 7. After failure (a) SH slope, (b) LH slope and laser sensors measurement (c) SH slope and (d) LH slope.

In the tests here, measurements made from SL and SSC tilt sensors as well as laser sensors were shown and compared. Here, for SL tilt sensors, only X-direction movement was measured whereas for SSC sensors, both X and Y direction movements were measured. In case of laser sensors, In case of laser sensors, slope surface movements measured were represented by S1, S2, S3 (from bottom upward) where as vertical and horizontal movements measured were represented by V1, V2 and H1, H2, respectively. In Figs. 6(a) and 6(b), movements of slope surface and slope top measured with laser sensors for SH and LH are shown. In case of Fig. 6(a), measurement of S1 and S2 were not good as the excavation reached the area of their set up positions after 6th cut onwards. In both the figures, almost no movement was seen at the beginning but the gradual increment with the increase in the steps of excavation could be measured from all the sensors. In case of SH slope, sharp increment was observed after 70 minutes. Similarly, in case of LH, sharp increment was observed after 95 minutes. In Figs. 7(a) and 7(b), measurements after 70 minutes for SH slope and after 95 minutes for LH slopes are shown. In both of those graphs, three curves were selected as shown in Fig. 7 and for each curve, inclination was measured. Change in the inclination (mm/min) for each curve is plotted in Figs. 8(a) and 8(b) for SH and LH slopes, respectively.

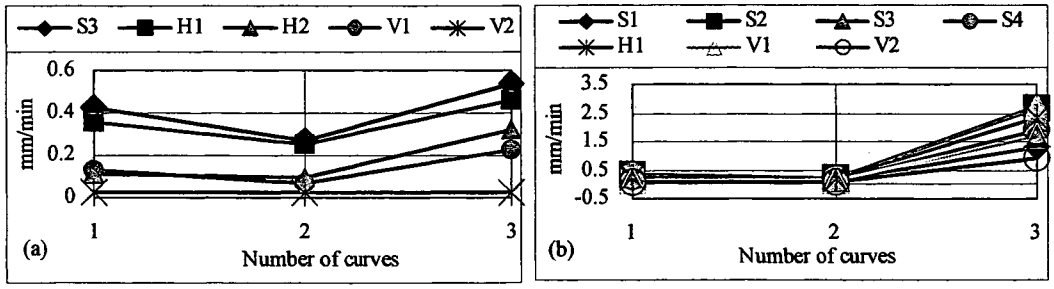

Figure 8. Measurement of laser sensors (a) SH slope and (b) LH slope.

In both the graphs, it could be observed that either the inclination of 2nd curve is little less than 1st curve or almost same where as the inclination of 3rd curve is comparatively very high. From this, it could be said that before reaching final failure, small decrement in inclination (or almost same) will take place after which sharp and final failure take place. This trend was observed in almost all the measurements made by laser sensors. One should be careful with this trend of change in increment. As seen from the graphs, the laser sensors which were set up near to the excavation portion, showed higher amount of change in the movement. Similarly, laser sensors set up toward the slope crest showed higher movement than those set up behind. Accordingly, S1 showed higher change in movement than those by S2, S3 and S4; S4 showing the minimum value. Similarly, on the slope top, H1 and V1 showed larger movement in comparison to H2 and V2, respectively.

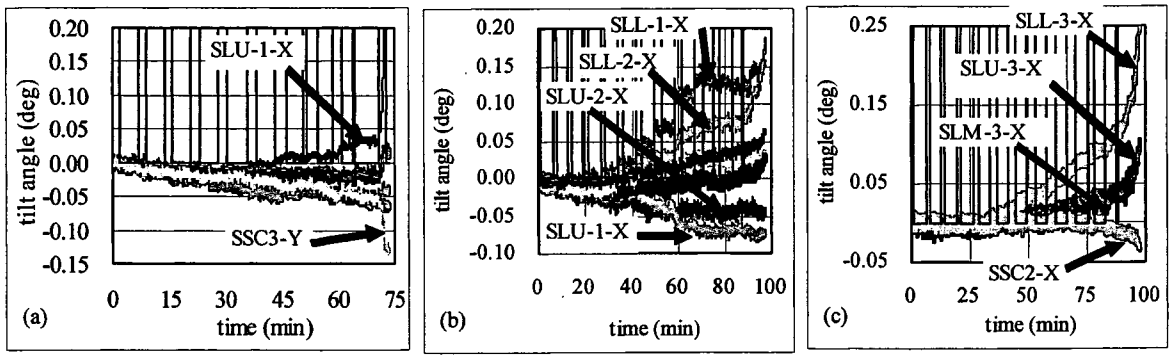

Figure 9. Measurements made from laser sensors (a) slope top (SH slope), (b) slope surface (LH slope) and (c) slope top (LH slope).

In Fig. 9, tilt angles measured on the slope surface and slope top for SH slope are shown. As the excavation reached the set up area of SSC-1 and SSC-2 tilt sensors after 6th cut, their data were not shown here. Hence, the measurement made on the slope top with SSC-3 (both X and Y movements) and SL-1 (X-direction only) and SL-2 (X-direction only) are shown. Although clear increments at the beginning of the excavation were not seen, change in the tilting angle could be seen with the increase in the steps of excavation. Just before the failure, i.e. after 70 minutes; sharp increment in the tilt angle was seen as those in laser sensors (Fig. 6(a)). Comparatively, the SL-1 and SSC-3 tilt sensors showed sharp change in their measurement just before the final failure. In case of SL-1, SLU-1 showed large tilting angle than SLL-1. For SSC-3 set up on the slope top (crest), positive movement along X direction and negative movement along Y direction, which was larger than X movement, were observed. From SSC-3 movement, it could be said that the slope had moved towards the right direction of the slope face during the failure. Similar failure pattern was seen during failure of the test also. Although no clear tensile crack or failure surface were appeared on the slope top, movements of SLU-1 and SLL-1 showed the possible measurement of slope movement of upper and inner layers. As shown in Table 2, SL-1 showed larger positive movement than SL-2 which showed very small negative movement only. Also, SLU-1-X showed larger movement than SLL-1-X, showing larger movement of upper layer than lower inner layer. Possible forward movement of the slope crest was hence occurred in the SH slope.

In Figs. 10(a) and (b), tilt angles measured for LH slope both by SL and SSC tilt sensors for the slope surface and slope top are shown, respectively. As in Fig. 7, here also, increments are not clear at the start with the increase in the step of excavation. But increment in tilt angle could be seen at the later stages of excavation; especially after 88 minutes of excavation, there was sharp increment in the tilt angle in all the cases. The increment became sharp when the elapsed time reached 95 minutes. In Fig. 10(a), comparing of the tilt angle measured by SL-1, SL-2 and SSC-1 are shown. SSC-1 showed positive X-direction movement only. Comparing the values of SL-1 and SL-2, all the SLL-1, SLM-1 showed higher positive values (X-direction) than SLL-2, SLM-2. In contrary, SLU-1 showed higher negative values (X-direction) than that by SLU-2. As SL-1 tilt sensor was set up closer to the excavation area, henceforth it showed the larger change in tilt angle than that by the SL-2 which was set up far away from the excavation area. It is to be pointed out here that the movement of all the sensors attached to SL-1 and SL-2 showed increment in tilt angles. This shows that the SL tilt sensor could measure the tilt angle of both upper and inner layers of the slope. As shown in Table 2, SL-1 and SL-2 both showed similar amount of movements; showing that whole the slope surface was moving forward, with the inner layer (SLL-1 and SLL-2) moving outward than the upper layers (SLU-1 and SLU-2). Since the inner layer movement angle

was larger than the upper layers, it could be said that SL type tilt sensors are suitable for the measurement of inner movements also. Also, comparative movement of the slope throughout the depth could be seen. In Fig. 10(b), measurement of tilt angle on the slope top by SL-3 and SSC-2 tilt sensors are shown. SSC-2 showed small change in negative value along X-direction whereas the tilt angles measured by SL-3 tilt sensor were all positive; SLL-3 showing the largest movement. As in the slope surface (SL-1 and SL-2), here also, SLL-3-X showed the maximum movement. This showed the movement of inner layer being more than the outer layer. As SL tilt sensor could measure the movement of inner as well as outer layers, it could be said that this SL tilt is more practical to use in the field than SSC tilt sensors.

Table 1. Properties of model tests.

Slope type	X	Y	SL-1	SL-2	SL-3
SH slope					
SSC-3	+0.03	-0.13			
SLU-X			+0.15	-0.04	
SLL-X			+0.02	-0.07	
LH slope					
SSC-1	+0.06				
SSC-2	-0.02				
SSC-3					
SLU-X			-0.07	-0.05	+0.09
SLM-X			+0.02	+0.02	+0.09
SLL-X			+0.15	+0.15	+0.23

To observe the nature of change in tilt angle just before failure, tilt angle measured by SL-1 for SH slope (after 70 minutes) and SL-2 and SL-3 in case of LH slopes (after 90 minutes) were divided into few curves as shown in Fig. 11(a) and 11(b), respectively, where the inclination of was changed. In case of SH slope little decrease in trend just before final and sharp increment could be seen for SLU-1-X. Laser displacement values (Fig. 11(a)) also showed the similar pattern. In case of LH slope, small increment in tilt angle just before that final and sharp increment could be seen for SLL-2-X and SLL-3-X and SLU-3-X. The trend of inclination of the curves is similar to those shown by the laser sensors although the amount of inclination was different. This might be due to the difference in the position of the tilt sensors and laser sensors. Here, the trend of change in the inclination before failure was not clear for all the sensors set up. This might be due to small time interval of 5 minutes allowed in between each cut which made it little difficult to measure the trend. With the allowance of longer waiting time, clear and distinct failure trend might be obtained.

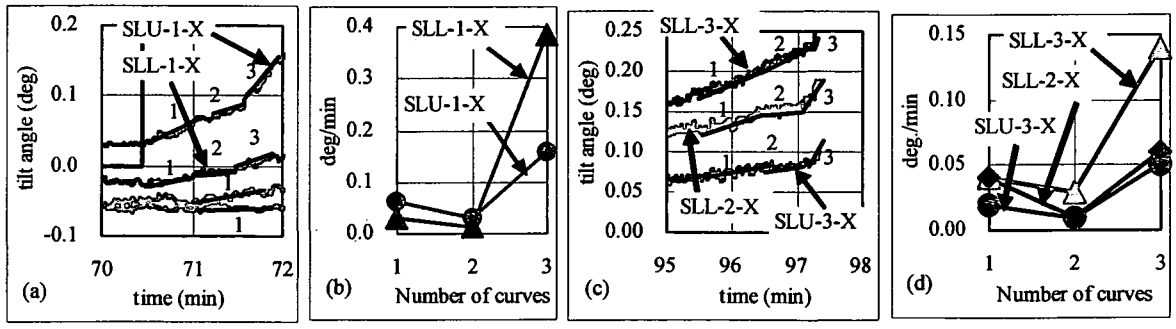

Figure 10. (a) Tilt angle, (b) deg/min curves for SH slope, and (c) tsilt angle and (d) deg/min for LH slope.

5 Conclusions

1. Change in tilt angle with the increment in excavation step could be seen with SSC and SL type tilt sensors.
2. SSC tilt sensor measured only upper layer movement. SL type tilt sensor could measure the tilt angle (movement) of outer and inner layers also. In case of SH, SLU-1 showed larger positive X-direction movement than that by SLL-1. In contrary, SLL-1, SLL-2 and SLL-3, all showed the maximum positive X-direction movement in case of LH slope, thereby showing the larger movement of inner layers of the slope.
3. Tilt angle measured by tilt sensors showed similar trend of increment as those measured by laser sensors. In both the cases, by observing the failure pattern just before the failure, it was observed that the increment in movement with the time decrease for a short time and then it suddenly increased and failed.

Acknowledgement

This work is partially carried out under the Health and Labor Sciences Research Grants of Ministry of Health, Labor and Welfare.

References

Aung, K.K., Rahardjo, H., Leong, E.C., Toll, D.G. 2001. Relationship between porosimetry measurement and soil-water characteristic curve for an unsaturated residual soil. Geotechnical and Geological Engineering. 19, 401-416.

Fredlund, D.G. and Rahardjo, H. 1993. Soil Mechanics for Unsaturated Soils. New York: John Wiley and Sons Inc.

Koseki, J., Matsuo, O. 1997. Liquefaction induced uplift of severe manholes and pipes. Proceedings of Third Asian Young Geotechnical Engineers Conference, Singapore, 549-557.

International Geotechnical Symposium "GEOTECHNICAL ENGINEERING FOR DISASTER PREVENTION & REDUCTION"
July 24-26, 2007, Yuzhno-Sakhalinsk, Russia

Physico-chemical on Mechanism of the Coefficient of Shear Resistance at the Residual State "tan ϕ_r" of Clay

M. Okawara[1], T. Hisatsune[2], T. Mitachi[3]

[1]Faculty of Engineering, Iwate University, Japan
[2]Graduate Student, Iwate University, Japan
[3]Graduate School of Engineering, Hokkaido University, Japan

Abstract

The coefficient of shear resistance at the residual state is a very important parameter in engineering, as usually used for landslide stability analysis. We examined the mechanism of the coefficient of residual state shear resistance "$tan\phi_r$". As a result of AFM measurement of shear surface it became clear that shear surface at the residual state was not a perfect flat, and also by CLSM observation, we found that the contact part of a glass board and a shear surface of clay was only partial contact. It indicates that the area actually touched was smaller than the apparent contact area. The "actual" contact area increased as the normal stress increased. While with FTIR measurement, adsorbed water on shear surface of cohesive soil decreased as the increase in normal stress. In conclusion, the coefficient of residual state shear resistance ($tan\phi_r$) of clay can be thought to be the coefficient originated in the increase in the actual contact area caused by the increase in the normal stress.

Keywords: *coefficient of shear resistance, residual state, clay, chemical and physical property*

1 Introduction

In various shear properties, the coefficient of shear resistance ($tan\phi$), which is an increase rate of the shear stress (τ) to an increase in the normal stress (σ), is an important parameter in engineering study. The states of the shear have peak state, fully softened state and residual state. Residual state is the steady state that the shear strength converges to a steady minimum value after being suffered a large shear deformation. It is known that the slip surface of landslide formed slicken side is in residual state. Mitachi et al. (2003) states clearly that the coefficient of shear resistance at the residual state ($tan\phi_r$) is the same as the coefficient of shear resistance of Hvorslev ($tan\phi_e$) which is thought to be the closest to the true coefficient of shear resistance at present. In other words, "the residual strength IS actual shear strength." Thus, we examined the mechanism of the coefficient of shear resistance at the residual state ($tan\phi_r$). A shear surface at the residual state is flat (Okawara et.al 2003), because particles on a shear surface become oriented after a large shear deformation. So, the shear phenomenon at the residual state can be understood as a friction phenomenon of two flat surfaces in a broad sense. In tribology, the definition of the coefficient of friction μ (F/P) is the ratio of the friction force(F) to the load(P) which is pressing two surfaces vertically. As mentioned above, the coefficient of shear resistance at the residual state ($tan\phi_r$) is the ratio of shear stress τ_r to vertical stress σ ($tan\phi = \tau_r/\sigma$). The coefficient of shear resistance($tan\phi$) is equivalent to the coefficient of friction (μ).The tribological reason for the existence of the coefficient of friction(μ) itself, or the friction force to the load, is that the increase in total actual contact area (Fig.1) is in proportion to the increase in normal stress (Holm,1958;Bowden & Tabor,1964; Greenwood & Williamson 1966). This study is to verify whether the same idea can be applied to the shear of clay. In particular, we focused on 3 points: ①Roughness of Shear Surface, ②Actual Contact Area, ③Spectroscopic Properties of Adsorbed Water.

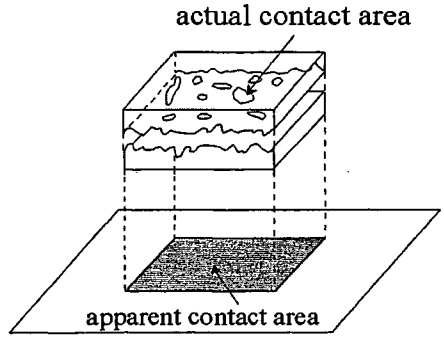

Figure 1. Conceptual diagram of actual contact area.

2 Sample and Experimental Methods

2.1 Sample

The sample used in the experiment was NSF- clay (New Snow Fine-clay). This clay is popular in geotechnical engineering field in Japan. Table 1 shows physical and mineralogical properties of NSF-clay. This clay is composed of a lot of Pyrophyllite and Quartz. Pyrophyllite is clay mineral and Quartz is mainly composed of sand, so NSF-clay is classified into cohesive soil. The specimen used for the observation of a shear surface was a remolded sample. To make this specimen, the deaerated water was added to powdered NSF-clay and remolded by a blender. Then it was put into a cylindrical acrylics cell and deaerated for 30 minutes, and preconsolidated for 7 days with the consolidation pressure of 150kPa.

Table 1. Chemical and Physical properties of NSF-clay.

Soil particle density : ρ_s	2.78g/cm^3
Plasticity index : I_P	41.7
Cation Exchange Capacity:CEC	24.5cmol/kg

2.2 Experimental Method

①Direct shear box test

The shear surface at the residual state made from a long displacement direct box shear test was used for various experiments (Fig.2). Conditions of direct box shear test were: Consolidated constant pressure condition, vertical stress =150kPa; shear displacement =200mm; shear speed =0.5mm/min.

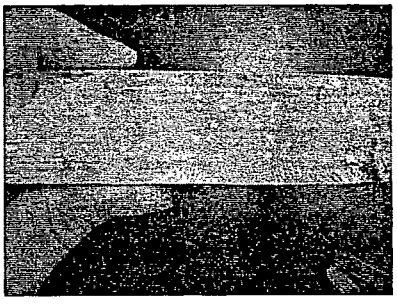

Figure 2. Shear surface at the residual state of NSF-clay.

②AFM (Atomic Force Microscope) Measurement

Asperity measurement and surface analysis of shear surface were done by using AFM (Atomic Force Microscope), namely, Veeco Nano Scope III (Fig.3a). The measurement range was 10 μ m × 10 μ m. The procedure was as follows. First, soon after the scanning started, 1 skip line was kept, and each parameter was adjusted so that the concave-convex waveform and error waveform of a reciprocating motion became the same. The sample surface was scanned by a tapping method (Fig.3b). Then surface analysis was done from the measured asperity image using the attached software, and the maximum height of the profile (R_{max}), arithmetic mean deviation of the profile (Ra), and increase rate of surface area (RIA) were calculated. Roughness was also quantified by using Ra and RIA. Ra indicates the arithmetic mean deviation of the profile. It is the total area of gray colored in Fig.4. RIA indicates the increase rate of surface area / against flat surface area. As roughness increases, both Ra and RIA also increase.

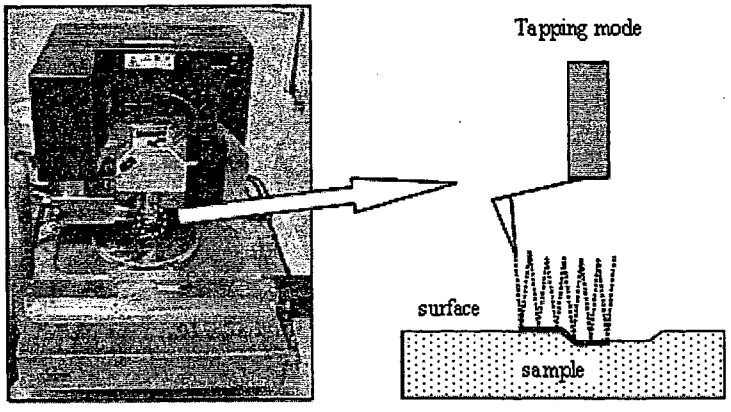

(a) Veeco Nano Scope III (b) measurement mode

Figure 3. Atomic Force Microscope.

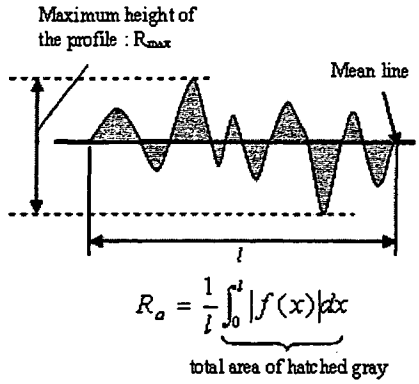

Figure 4. Index of roughness: R_{max}, R_a.

③ CLSM (Confocal Laser Scan Microscope) Observation

The confocal laser scan microscope was used for observing a shear interface. CLSM used for this observation was Bio Rad MRC-1024 (Fig.5a). A confocal laser scan microscope irradiates a sample, detects the light or fluorescence reflected from the sample, and with these data, computer makes the image of the sample. The advantage of this microscope is that it only measures the light from the focal plane that passed through a small hole called a "pinhole" (Fig.5b). By excluding unnecessary light from the upper and lower sides, comparing with the conventional microscopes, its resolution is improved about 1.4 times, so that clear pictures can be expected. Furthermore, even if a sample is thick, we can obtain optical tomograms of the arbitrary depth because a laser can reach deep. An observation was made on a contact plane of a shear surface and a glass. The shear surface formed by the direct box shear test was cut into a size to fit with an observation unit. It was then placed and stuck to a tempered glass which was attached at the lower part of the unit. From the glass side, laser was beamed and the contact part of a glass and a shear surface was observed. The conditions of the observation were, reflection, pinhole diameter:1mm, laser strength:3%, image averaging process:5times.

Moreover, a load unit was used to observe the contact surface when adding normal stress. Figure 6 shows the loading method. The normal stress was added by weights.

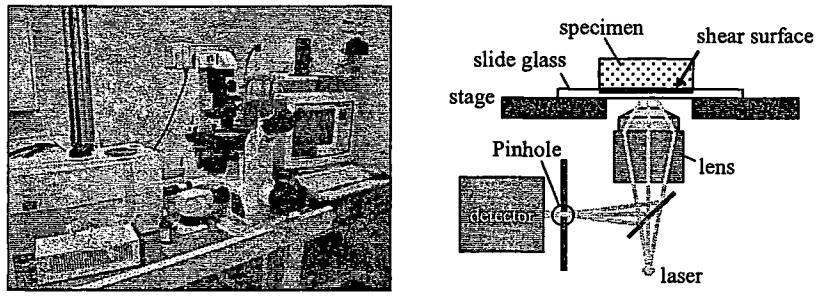

(a) Bio-rad MRC 1024 (b) observation system

Figure 5. Confocal Laser Scan Microscope (CLSM) .

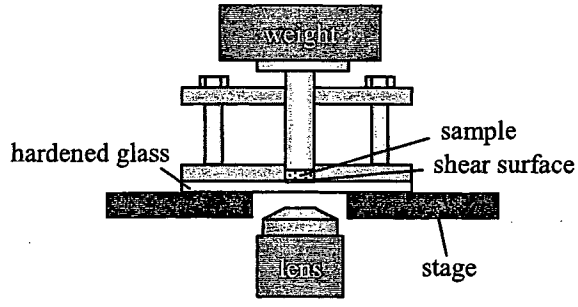

Figure 6. Overview of a pressure unit.

④FTIR (Fourier Transform Infrared Spectrometer) Analysis

In order to clarify the spectroscopic properties of the adsorbed water of a shear surface, it was measured by FTIR (Fourier Transform Infrared Spectrometer). Microscopic-FTIR used for this measurement was JESCO VIR-9500, IR-30 (Fig.7a). The measurement was done by ATR that sticks a prism to a sample surface. Microscopic- FTIR does a great job especially when it comes to a local analysis of a sample surface, and also or a very small quantity of or minute samples. As to this experiment, the diameter was 250 μ m, and measurement depth was 250nm - 2000nm. Background measurement was done first. Subsequently, to perform an infrared spectrum measurement, the shear surface of a sample was touched by a prism of ATR equipment. At this time, the contact pressure of the sample surface and the prism was measured by a small load cell under the sample (Fig.7b). Measurement wavenumber domains :